Tonkie Khimicheskie Tekhnologii = Fine Chemical Technologies.
2025;20(1):63–74 ISSN 2686-7575 (Online)

UDC 544.032
https://doi.org/10.32362/2410-6593-2025-20-1-63-74
EDN XZSYPF

RESEARCH ARTICLE

Structure and properties of Li ferrite synthesized from Fe_2O_3–Li_2CO_3–Sm_2O_3 powders

Elena N. Lysenko✉, **Vitaly A. Vlasov, Yuliya S. Elkina, Anatoly P. Surzhikov**

National Research Tomsk Polytechnic University, Tomsk, 634050 Russia

✉ *Corresponding author, e-mail: lysenkoen@tpu.ru*

Abstract

Objectives. To study the structure and properties of lithium ferrites obtained by preliminary solid-phase synthesis of samples based on Fe_2O_3–Li_2CO_3–Sm_2O_3 powder mixtures having various concentrations of samarium oxide (0, 4.7, and 14.7 wt %) at 900°C and their subsequent high-temperature sintering at 1150°C.

Methods. The structural and morphological characteristics of the synthesized and sintered samples were studied by X-ray powder diffraction analysis, scanning electron microscopy, thermogravimetric analysis, and differential scanning calorimetry.

Results. The preliminary synthesis gives a two-phase composite structure containing unsubstituted lithium ferrite $Li_{0.5}Fe_{2.5}O_4$ having a spinel structure and a perovskite-like $SmFeO_3$ phase. An increase in the Sm_2O_3 content from 4.7 to 14.7 wt % in the initial Fe_2O_3–Li_2CO_3–Sm_2O_3 mixture leads to an increase in the amount of the secondary $SmFeO_3$ phase in the synthesized samples from 4.9 to 18.2 wt %. The high Curie temperature values (631–632°C) and obtained values of the enthalpy of the α→β phase transitions in lithium ferrite indicate that the main product in all synthesized samples is the ordered α-$Li_{0.5}Fe_{2.5}O_4$ phase. Subsequent sintering at elevated temperatures leads to a decrease in the $SmFeO_3$ phase content to 3.8 and 16.5 wt % and to an increase in the content of the lithium ferrite phase. The sample not modified with samarium contains a significant amount of the disordered β-$Li_{0.5}Fe_{2.5}O_4$ phase, as confirmed by the reduced values of the Curie temperature and phase transition enthalpy. The density of such a sample is 4.4 g/cm^3. The introduction of samarium ions leads to the preservation of the ordered α-$Li_{0.5}Fe_{2.5}O_4$ phase during sintering. The density of the sintered samples decreases to 4.3 and 4.1 g/cm^3 with an increase in the concentration of samarium oxide introduced at the synthesis stage to 4.7 and 14.7 wt %, respectively.

Conclusions. The introduction of samarium oxide to low concentrations (up to 4.7 wt %) during ferrite synthesis leads to the formation of a two-phase composite structure during sintering, which mainly consists of an unsubstituted lithium ferrite phase having more regular polyhedral grains and a low content of the secondary perovskite-like phase. The formation of the secondary phase, whose properties differ from those of ferrite, along with the characteristics obtained for such samples, which include a slight decrease in density while maintaining a high Curie temperature corresponding to the main magnetic phase, make ferrites modified with low concentrations of rare earth elements promising for further study of their electromagnetic properties in the microwave range.

Keywords

lithium ferrite, samarium oxide, perovskite, microstructure, solid-phase synthesis, sintering

Submitted: 10.09.2024
Revised: 09.11.2024
Accepted: 25.12.2024

For citation

Lysenko E.N., Vlasov V.A., Elkina Yu.S., Surzhikov A.P. Structure and properties of Li ferrite synthesized from Fe_2O_3–Li_2CO_3–Sm_2O_3 powders. *Tonk. Khim. Tekhnol. = Fine Chem. Technol.* 2025;20(1):63–74. https://doi.org/10.32362/2410-6593-2025-20-1-63-74

НАУЧНАЯ СТАТЬЯ

Структура и свойства Li феррита, синтезированного из порошков Fe_2O_3–Li_2CO_3–Sm_2O_3

Е.Н. Лысенко✉, **В.А. Власов, Ю.С. Елькина, А.П. Суржиков**

Национальный исследовательский Томский политехнический университет, Томск, 634050 Россия

✉ *Автор для переписки, e-mail: lysenkoen@tpu.ru*

Аннотация

Цели. Исследование структуры и свойств литиевых ферритов, полученных путем предварительного твердофазного синтеза образцов на основе порошковых смесей Fe_2O_3–Li_2CO_3–Sm_2O_3 с различной концентрацией оксида самария (0, 4.7, 14.7 мас. %) при 900°C и последующего их высокотемпературного спекания при 1150°C.

Методы. Структурные и морфологические характеристики синтезированных и спеченных образцов исследованы методами рентгенофазового и термогравиметрического анализов, дифференциально-сканирующей калориметрии и сканирующей электронной микроскопии.

Результаты. В результате предварительного синтеза происходит образование двухфазной композиционной структуры, содержащей незамещенный литиевый феррит $Li_{0.5}Fe_{2.5}O_4$ со структурой шпинели и перовскитоподобную фазу $SmFeO_3$. Увеличение содержания Sm_2O_3 с 4.7 до 14.7 мас. % в исходной смеси Fe_2O_3–Li_2CO_3–Sm_2O_3 приводит к увеличению во время синтеза количества вторичной фазы $SmFeO_3$ с 4.9 до 18.2 мас. % в образцах. Высокие значения температуры Кюри, равные 631–632°C, а также полученные значения энтальпии фазовых переходов α→β в литиевом феррите свидетельствуют об основном образовании упорядоченной α-фазы $Li_{0.5}Fe_{2.5}O_4$ во всех синтезированных образцах. Последующее спекание при повышенной температуре приводит к уменьшению содержания фазы $SmFeO_3$ и увеличению фазы литиевого феррита. При этом образец, не модифицированный самарием, содержит значительное количество разупорядоченной β-фазы $Li_{0.5}Fe_{2.5}O_4$, что было подтверждено заниженными значениями температуры Кюри и энтальпии фазового перехода. Плотность такого образца 4.4 г/см^3. Введение ионов самария приводит к сохранению во время спекания упорядоченной α-фазы $Li_{0.5}Fe_{2.5}O_4$. При этом плотность спеченных образцов уменьшилась до 4.3 и 4.1 г/см^3 с увеличением концентрации вводимого на этапе синтеза оксида самария соответственно до 4.7 и 14.7 мас. %.

Выводы. Введение малых концентраций оксида самария (до 4.7 мас. %) при синтезе феррита приводит к формированию во время спекания двухфазной композиционной структуры, характеризующейся основным содержанием незамещенной литиевой ферритовой фазы с более правильными многогранными зернами и небольшим содержанием вторичной перовскитоподобной фазы. Формирование вторичной фазы, которая имеет отличные от феррита свойства, а также полученные характеристики для таких образцов, включающие незначительное уменьшение их плотности с сохранением высокого значения температуры Кюри, соответствующей основной магнитной фазе, делают ферриты, модифицированные низкими концентрациями редкоземельных элементов, перспективными для дальнейшего изучения их электромагнитных свойств в сверхвысокочастотном диапазоне.

Ключевые слова

литиевый феррит, оксид самария, перовскит, микроструктура, твердофазный синтез, спекание

Поступила: 10.09.2024
Доработана: 09.11.2024
Принята в печать: 25.12.2024

Для цитирования

Лысенко Е.Н., Власов В.А., Елькина Ю.С., Суржиков А.П. Структура и свойства Li феррита, синтезированного из порошков Fe_2O_3–Li_2CO_3–Sm_2O_3. *Тонкие химические технологии*. 2025;20(1):63–74. https://doi.org/10.32362/2410-6593-2025-20-1-63-74

INTRODUCTION

Ferrites having a spinel structure are widely used in microwave devices, such as isolators, circulators, phase shifters, and absorbers [1–5], as well as in magnetically controlled photocatalysts [6]. The tightening of operating conditions for devices based on such ferrites determines the importance of research into the creation of new ferrite materials offering a required set of properties, as well as the development and improvement of their production technology.

Unsubstituted lithium ferrite $Li_{0.5}Fe_{2.5}O_4$ (or $LiFe_5O_8$), which has a high Curie temperature and a high saturation magnetization, is successfully used in practice, e.g., as ferrite cores in memory devices, for power conversion in electronics, in antennas and high-speed digital tapes [7, 8]. However, the use of lithium ferrites in microwave technology is limited by their excessive magnetic and dielectric losses. Therefore, lithium-containing ferrites often have more complex compositions [9–12] associated lower values of losses, anisotropy, and coercivity, as well as higher density, etc.

Recently, the properties of ferrites with rare-earth elements (REEs) have been actively studied. Many scientists explored the effect of various REEs on the properties of ferrites of Li [13], Ni [14–16], Co [17, 18], Li–Ni [19–21], Ni–Zn [22], Ni–Mn [23], Co–Mn [24], and Cu–Co [25]. At the same time, it has been shown [14, 16, 20, 22, 24, 25] that the properties of ferrites can be modified by substituting REE ions in the ferrite structure. For this purpose, various chemical synthesis methods are used, such as the sol–gel method [14, 22, 25], citrate method [16], coprecipitation [18], microemulsion method [20], hydrothermal method [24], etc. In other works [13, 15, 17, 21, 23], when producing ferrites by various methods that include the widespread solid-phase synthesis method, it has been shown that the addition of REEs simultaneously with substituted ferrite phases leads to the formation of a small amount of secondary perovskite-like phases based on REEs. Such phases can have a significant effect on the properties of the synthesized ferrites. However, there is insufficient data on the production of lithium ferrites with REEs using preliminary synthesis of ferrites by the solid-phase method and subsequent high-temperature sintering.

Our previous studies showed [26] that the solid-phase synthesis of lithium ferrites from Fe_2O_3–Li_2CO_3–Sm_2O_3 mixtures, regardless of the conditions of mechanical activation of the initial powders, gives a two-phase product consisting of unsubstituted lithium ferrite $Li_{0.5}Fe_{2.5}O_4$ and $SmFeO_3$. This work is aimed at studying the structure and properties of lithium ferrite produced using a two-stage technology based on preliminary solid-phase synthesis of ferrite with the addition of REE (Sm_2O_3) at various concentrations and subsequent high-temperature sintering to obtain ferrite ceramics. The process conditions for the synthesis and sintering of this group of ferrites are also considered in detail.

EXPERIMENTAL

The production of the ferrites under study (Fig. 1) is based on the mechanical mixing of oxide powders and carbonate powders. Let us consider in more detail the process stages of synthesis and sintering of the ferrite under study.

Figure 1a presents the stage of the preliminary synthesis (ferritization) of lithium ferrite. Prior to their synthesis, powders of the initial reagents Li_2CO_3 (special purity grade 20-2, *Vekton*, Russia), Fe_2O_3 (analytical purity grade, *Vekton*, Russia), and Sm_2O_3 (99.99%, *MOS International Co*., China) were dried in a laboratory oven at a temperature of 200°C for 180 min and then weighed on an AUW-D scale (*Shimadzu*, Japan) to obtain weight proportions in accordance with the proposed formulas:

$$Li_2CO_3 + 5Fe_2O_3 \rightarrow \rightarrow 4Li_{0.5}Fe_{2.5}O_4 + CO_2 \text{ (sample N0)}, \quad (1)$$

$$Li_2CO_3 + 4.88Fe_2O_3 + 0.12Sm_2O_3 \rightarrow \rightarrow 4Li_{0.5}Sm_{0.06}Fe_{2.44}O_4 + CO_2 \text{ (sample N1)}, \quad (2)$$

$$Li_2CO_3 + 4.6Fe_2O_3 + 0.4Sm_2O_3 \rightarrow \rightarrow 4Li_{0.5}Sm_{0.2}Fe_{2.3}O_4 + CO_2 \text{ (sample N2)}. \quad (3)$$

Next, the initial reagents were mixed to obtain a Fe_2O_3–Li_2CO_3–Sm_2O_3 powder mixture in weight ratios of 91.5 : 8.5 : 0 (sample N0), 87.1 : 8.2 : 4.7 (sample N1), and 77.5 : 7.8 : 14.7 (sample N2) in two steps.

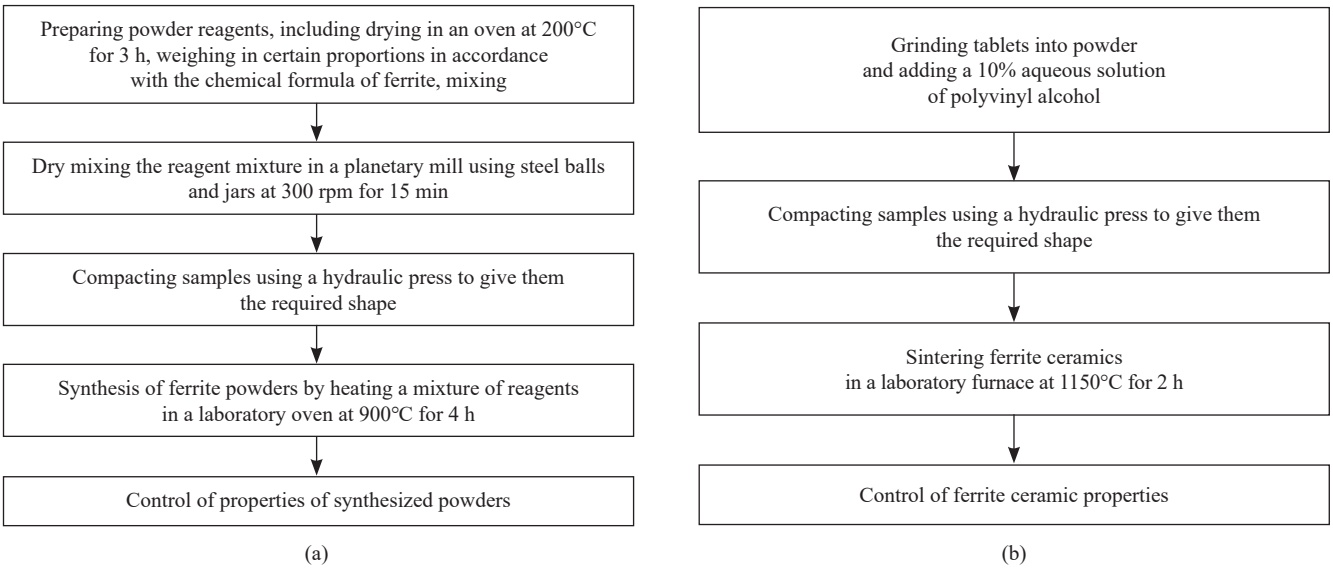

Fig. 1. Process flow diagrams for the (a) synthesis and (b) sintering of ferrites

At the first step, the powders were gradually mixed by rubbing through fine steel sieves with a cell size of 100 μm. At the second step, for the mixing to be more thorough and for the obtained mixture to be more uniform in volume, the powders were mechanically ground in a planetary ball mill with steel grinding jars and balls at 300 rpm for 15 min.

Next, the samples were compacted into 2-mm-thick pellets 15 mm in diameter to create closer contacts between particles and thus encourage the synthesis reaction to occur better and more completely. The samples were synthesized in a laboratory furnace in air at a temperature of 900°C for a holding time of 240 min. Following synthesis, the phase composition and Curie temperature of the obtained samples were determined.

Figure 1b presents the stage of the high-temperature sintering of lithium ferrite. First, the synthesized samples were ground again and stirred. Then, the samples were recompacted into pellets of the described shape.

The compactibility of powders is typically improved by adding various binders (plasticizers) to promote mutual adhesion of individual particles, followed grinding the mass in a mortar. The main requirement for all binders is that they should be completely removed from the compacted parts when heating to 600°C. In this work, a 10% aqueous solution of polyvinyl alcohol was used as a binder.

The samples were compacted in a hydraulic press using steel molds. It is known that the pressing pressure depends on the pellet size and the design of the mold. In the work, the compaction parameters of the samples were selected experimentally: pressing pressure—200 MPa; pressing time—3 min. The set pressure was 20% lower than the maximum pressure at which the sample has not yet delaminated.

The molded samples were sintered at a temperature of 1150°C for 120 min. High-temperature sintering in the furnace consisted of three steps: heating at a certain rate to the sintering temperature, isothermal holding at this temperature, and cooling. The heating and cooling rate was 5 deg/min.

The purpose of the sintering stage is to obtain ferrite products with a certain set of properties. Sintering is known to be accompanied by recrystallization processes consisting in the formation and migration of intergranular boundaries. This forms a microstructure that largely determines the properties of the resulting ferrites. Thus, the purpose of the high-temperature sintering in this work is to ensure the formation of lithium ferrite of cubic structure having a certain grain size and porosity, as well as minimum internal stresses in crystallites at a given chemical composition.

The sintered samples were sent for analysis of their phase composition, microstructure, and Curie temperature. X-ray powder diffraction analysis (XRD) of the samples was carried out with an ARL X'TRA X-ray diffractometer (*Thermo Fisher Scientific*, Switzerland). Phases were identified using the PDF-4+ powder database of the International Center for Diffraction Data (ICDD[1]). The microstructure of the samples was studied with a TM-3000 scanning electron microscope (*Hitachi*, Japan). The average grain size was calculated from scanning electron microscopy (SEM) results. The density of the samples was determined by hydrostatic weighing. The Curie temperature of lithium ferrites and phase transitions in them were studied, respectively, by thermogravimetry (TG) with the application of an external magnetic field (thermomagnetometry), as well as differential scanning calorimetry (DSC) using an STA 449C Jupiter thermal analyzer (*Netzsch*, Germany).

RESULTS AND DISCUSSION

The results of X-ray powder diffraction analysis (Fig. 2) showed that the preliminary synthesis and high-temperature sintering of REE-free samples (sample N0) produce a spinel magnetic phase. The X-ray powder diffraction patterns of sample N0 correspond to the ordered phase α-$Li_{0.5}Fe_{2.5}O_4$ (PDF No. 04-015-5965) and the disordered phase β-$Li_{0.5}Fe_{2.5}O_4$ (PDF No. 00-017-0114) with cubic space groups (*Fd*3*m*).

In samples N1 and N2, a secondary crystalline phase identified as $SmFeO_3$ (PDF No. 00-039-1490) is formed along with the spinel phase. $SmFeO_3$ is an orthoferrite with a perovskite-like crystal structure and orthorhombic space group (*Pnma*).

Thus, initial reactions (2) and (3) in samples N1 and N2 have different forms. In the case of the formation of the $Li_{0.5}Fe_{2.5}O_4$ and $SmFeO_3$ phases, the excess lithium, which is initially loaded at the stage of mixing the initial reagents, is released in the reaction products. Previously [27], it was detected that part of the lithium oxide formed by the decomposition of lithium carbonate during the synthesis of lithium ferrites sublimates at a temperature above 900°C and volatilizes together with oxygen. Therefore, the interaction reactions in the Fe_2O_3–Li_2CO_3–Sm_2O_3 system can proceed in samples N1 and N2 according to the following equations, respectively:

$$Li_2CO_3 + 4.88Fe_2O_3 + 0.12Sm_2O_3 \rightarrow \\ \rightarrow 3.808Li_{0.5}Fe_{2.5}O_4 + 0.24SmFeO_3 + 0.048Li_2O + CO_2, \quad (4)$$

$$Li_2CO_3 + 4.6Fe_2O_3 + 0.4Sm_2O_3 \rightarrow \\ \rightarrow 3.36Li_{0.5}Fe_{2.5}O_4 + 0.4SmFeO_3 + 0.16Li_2O + CO_2. \quad (5)$$

[1] URL: http://www.icdd.com. Accessed October 3, 2023.

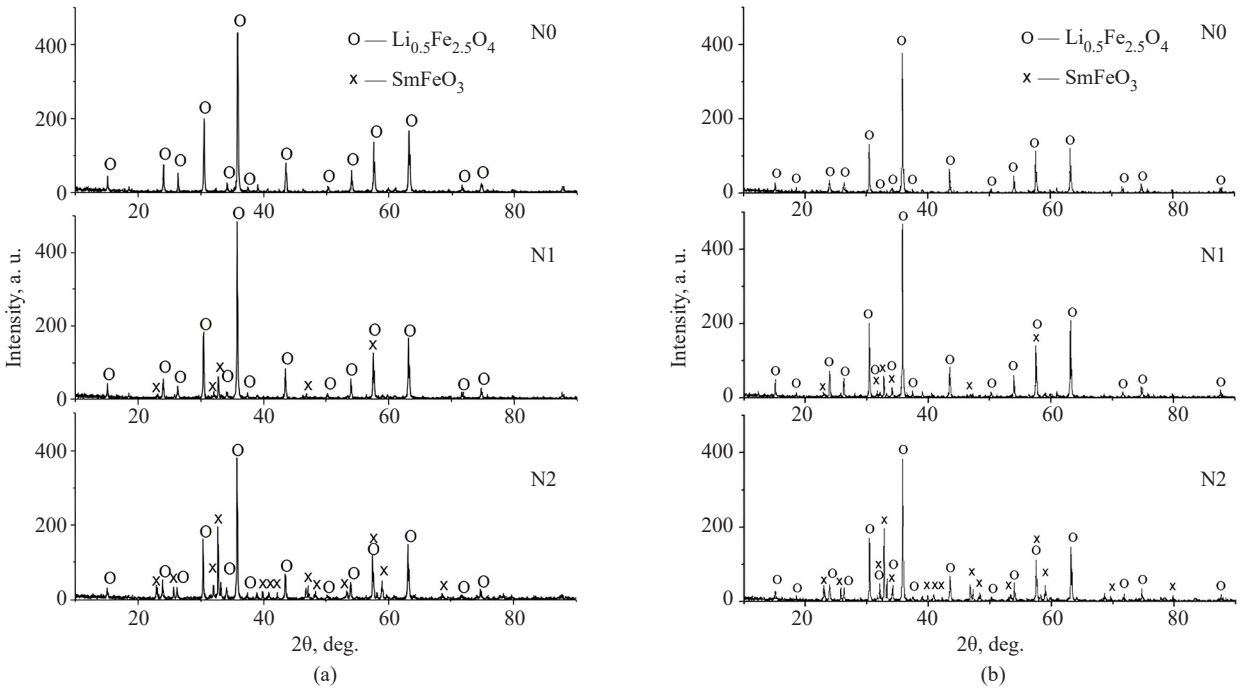

Fig. 2. X-ray powder diffraction analysis of (a) synthesized and (b) sintered ferrites N0, N1, and N2

Figure 3 shows the crystal lattices of the identified phases as generated by the PowderCell 2.4 powder pattern calculation program[2]. The quantitative contents of the synthesized phases presented in Table 1 depend on the concentration of the introduced Sm_2O_3. An increase in the Sm_2O_3 content from 4.7 (sample N1) to 14.7 wt % (sample N2) in the Fe_2O_3–Li_2CO_3–Sm_2O_3 mixture leads to an increase in the concentration C of the secondary phase $SmFeO_3$ in the synthesized samples from 4.9 to 18.2 wt %. Accordingly, the content of lithium ferrite decreases (Table 1).

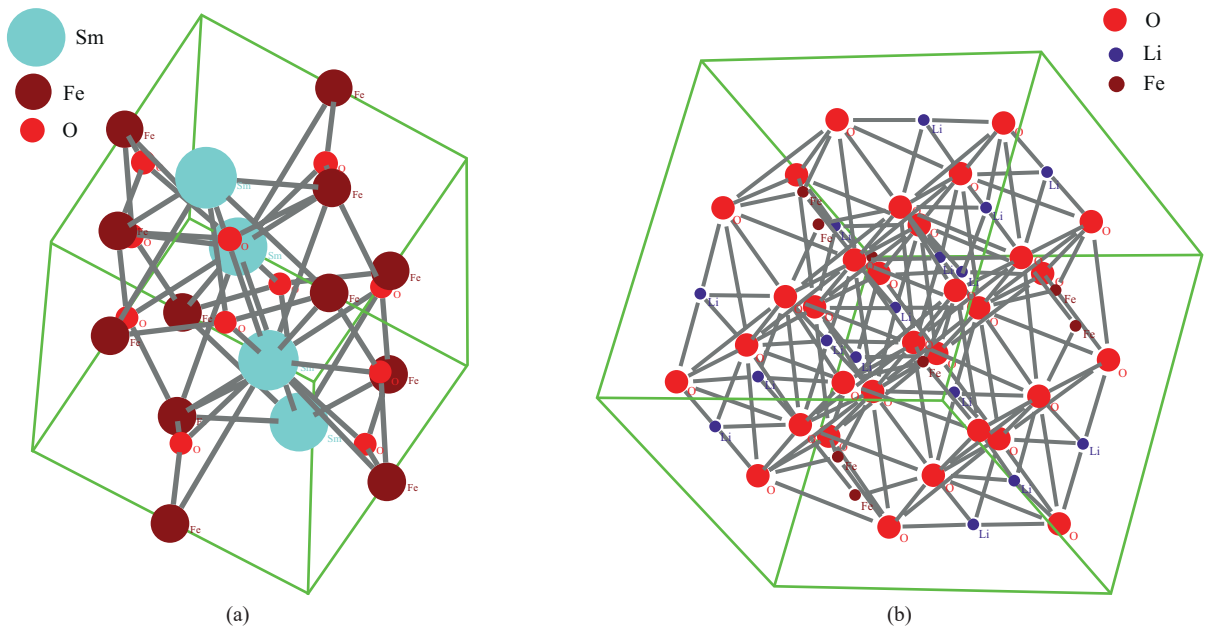

Fig. 3. Crystal lattices of (a) $SmFeO_3$ and (b) $Li_{0.5}Fe_{2.5}O_4$

[2] Kraus W., Nolze G. POWDERCELL – a program for representation and manipulation of crystal structures and calculations of the resulting X-ray powder patterns. *J. Appl. Cryst.* 1996:29;301–303.

Table 1. Phase composition and properties of synthesized ferrites

Sample	Phase composition	Lattice parameter, Å	*C*, wt %	T_C, °C
N0	$Li_{0.5}Fe_{2.5}O_4$	$a = b = c = 8.329$ (±0.002)	100.0	632.4
N1	$Li_{0.5}Fe_{2.5}O_4$	$a = b = c = 8.330$ (±0.002)	95.1	632.5
	$SmFeO_3$	$a = 5.592$ (±0.002); $b = 7.706$ (±0.003); $c = 5.400$ (±0.003)	4.9	
N2	$Li_{0.5}Fe_{2.5}O_4$	$a = b = c = 8.331$ (±0.002)	81.8	631.9
	$SmFeO_3$	$a = 5.594$ (±0.002); $b = 7.705$ (±0.003); $c = 5.400$ (±0.003)	18.2	

Note: C is the concentration; T_C is the Curie temperature.

In the sintered samples (Fig. 2b; Table 2), the concentration of the $Li_{0.5}Fe_{2.5}O_4$ phase slightly increases, while the amount of the secondary phase $SmFeO_3$ decreases in comparison with the synthesized samples. The lattice parameters obtained in this work are in satisfactory agreement with the literature data [27].

The quantitative analysis of the phase content of two polymorphs of $Li_{0.5}Fe_{2.5}O_4$ (α and β) using the X-ray powder diffraction patterns recorded in this study is complicated by the angular coincidences of these reflections (close lattice parameters). Unlike β-$Li_{0.5}Fe_{2.5}O_4$, the α polymorph has superstructural reflections at $2\theta \approx 15°$ (110), 23.9° (210), and 26.2° (211). The presence of high-intensity superstructural reflections in the diffraction patterns indicates ordering of the lithium spinel structure. Therefore, we assessed and explained the obtained results by analyzing the changes in the intensities of the superstructural reflections (110), (210), and (211) (Table 3). According to these data, the intensities of superstructure reflections for samples N0 and N1 are high following preliminary synthesis, their sum being greater than that for sample N2. This shows a large amount of α-$Li_{0.5}Fe_{2.5}O_4$ in these samples, whereas the low intensities for N2 samples are likely to be due to an increase in the amount of the perovskite phase.

The intensities of superstructure reflections for sintered sample N0 are low, their sum being smaller than that for samples N1 and N2. This indicates the presence of a large amount of the β-$Li_{0.5}Fe_{2.5}O_4$ phase, which could have formed during high-temperature sintering due to a violation of the stoichiometric composition in oxygen within the single-phase composition [28].

Table 2. Phase composition and properties of sintered ferrites

Sample	Phase composition	Lattice parameter, Å	*C*, wt %	*D*, μm	ρ, g/cm^3	T_C, °C
N0	$Li_{0.5}Fe_{2.5}O_4$	$a = b = c = 8.332$ (±0.002)	100.0	7.9	4.4	622.6
N1	$Li_{0.5}Fe_{2.5}O_4$	$a = b = c = 8.327$ (±0.002)	96.2	2.9	4.3	628.5
	$SmFeO_3$	$a = 5.594$ (±0.002); $b = 7.706$ (±0.003); $c = 5.401$ (±0.003)	3.8			
N2	$Li_{0.5}Fe_{2.5}O_4$	$a = b = c = 8.329$ (±0.002)	83.5	1.7	4.1	630.0
	$SmFeO_3$	$a = 5.592$ (±0.002); $b = 7.707$ (±0.003); $c = 5.400$ (±0.003)	16.5			

Note: C is the concentration, *D* is the average grain size, ρ is the density, and T_C is the Curie temperature.

Table 3. Intensities of the maxima of superstructural reflections (110), (210), and (211) for α-$Li_{0.5}Fe_{2.5}O_4$

Sample	Synthesis				Sintering			
	(110)	(210)	(211)	∑	(110)	(210)	(211)	∑
N0	51	79	66	196	30	35	29	94
N1	54	83	58	195	50	73	53	176
N2	27	36	30	93	29	45	37	111

The SEM results (Fig. 4) demonstrate different particle morphology in the studied samples. A structure having high density (ρ = 4.4 g/cm^3, Table 2), low porosity, and large irregular shaped grains (average grain size D = 7.9 μm, Table 2) is characteristic of lithium ferrite without the addition of REE.

The results of scanning electron microscopy of samples N1 and N2 confirm the previous conclusions about the formation of a two-phase product during the production of ferrite from the Fe_2O_3–Li_2CO_3–Sm_2O_3 powder mixture. In the SEM images, two shades can be clearly distinguished, one being the main spinel ferrite phase (gray), while the other represents the secondary phase $SmFeO_3$ (white). The presence of the secondary phase leads to a decrease in the density of the samples during sintering (Table 2), especially at high concentrations of introduced Sm_2O_3, as well as to a decrease in the average grain size. At the same time, sample N1 with a small addition of REE has ferrite grains having a more regular polyhedral shape characteristic of lithium ferrite.

The peaks in the DSC curves (Fig. 5) due to the α→β phase transition in $Li_{0.5}Fe_{2.5}O_4$ confirm the formation of a certain amount of ordered α-phase of lithium ferrite during synthesis and sintering. The areas of these peaks depend on the amount of lithium ferrite. The enthalpy of the α→β transition at a high content of α-$Li_{0.5}Fe_{2.5}O_4$ is known to be 12–13 J/g [29]. In the preliminary synthesis of ferrites, the DSC peak areas are approximately within this range of enthalpies for all samples (Fig. 5a). The Curie temperature range of ~630–632°C obtained from derivative TG curves was reported [30–32] to correspond to unsubstituted lithium ferrite with the chemical formula α-$Li_{0.5}Fe_{2.5}O_4$.

The high-temperature sintering of samples without the addition of REE in a dilatometer leads to an increase in the weight step in the TG measurements, which is related to the high magnetization of the obtained samples (Fig. 5b). At the same time, the Curie temperature is reduced (622°C), which may be a consequence of a violation of the stoichiometric composition of the samples due to the release of lithium and oxygen to form a disordered β-$Li_{0.5}Fe_{2.5}O_4$ phase. The excessively low Curie temperature for β-$Li_{0.5}Fe_{2.5}O_4$ is confirmed by literature data [33]. The small area (2 J/g) of the DSC peak for samples N0 also indicates a high content of the disordered β phase.

The area of the DSC peaks for samples N1 and N2 (Fig. 5) is 12.2 and 11.6 J/g, which values are close to the enthalpy of the α→β transformation in lithium ferrite. For sintered sample N2, which contains a large amount of REE, the weight step in the TG measurements decreases due to a decrease in the concentration of the magnetic phase of lithium ferrite. In the studied samples,

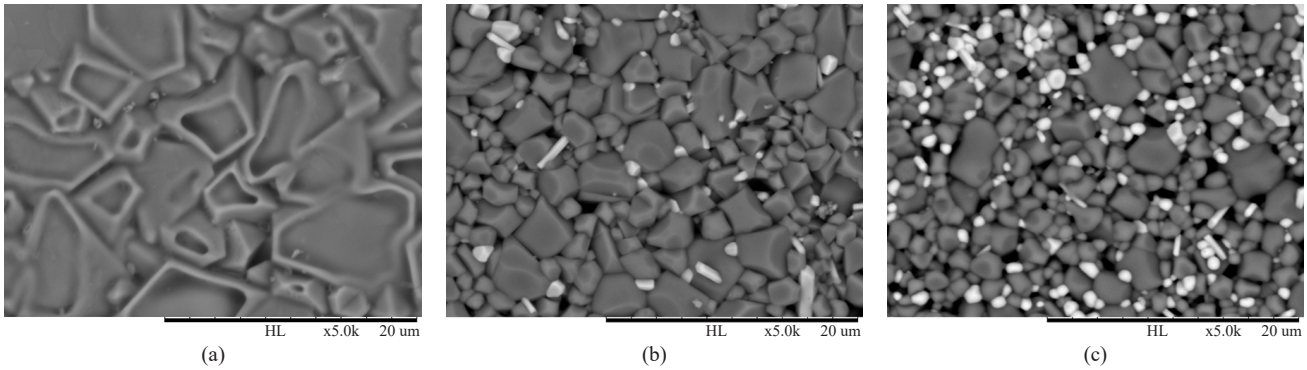

(a) (b) (c)

Fig. 4. SEM images of sintered samples: (a) N0, (b) N1, and (c) N2

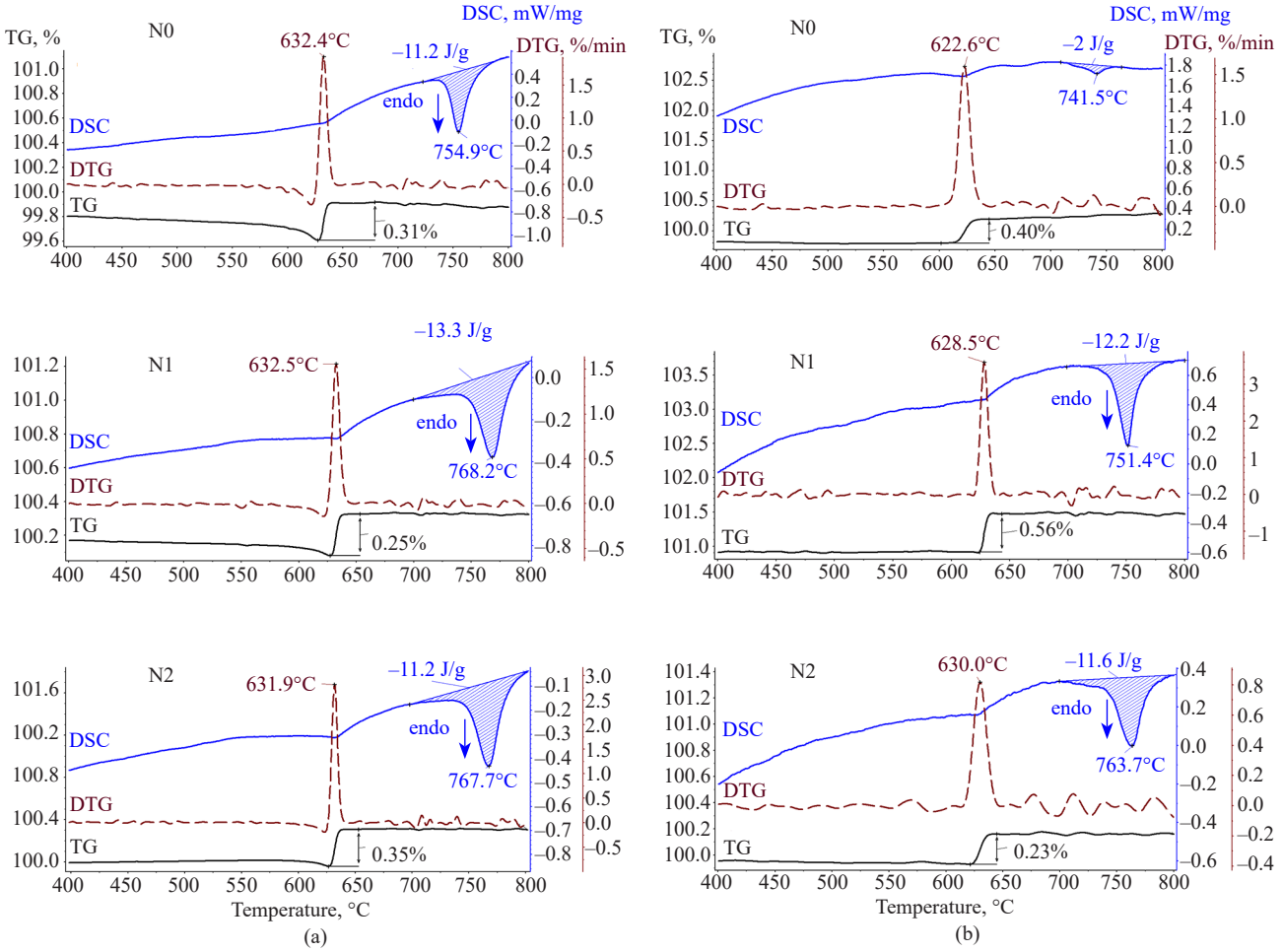

Fig. 5. Thermomagnetometric and differential scanning calorimetric analyzes of samples N0, N1, and N2 obtained by (a) preliminary synthesis and (b) sintering

neither X-ray powder diffraction nor thermal analyses revealed the formation of substituted lithium ferrite phases during preliminary synthesis or during high-temperature sintering.

CONCLUSIONS

In this work, the structure and properties of lithium ferrite obtained by preliminary solid-phase synthesis and subsequent high-temperature sintering from the initial reagents Fe_2O_3–Li_2CO_3–Sm_2O_3 were studied by XRD, TG, DSC and SEM analyses. The interaction between the initial reagents was shown to lead to the formation of a product consisting mainly of lithium ferrite $Li_{0.5}Fe_{2.5}O_4$ (α and β polymorphs) having a spinel structure, while the $SmFeO_3$ phase had a perovskite-like structure. The quantity of the latter increased with an increase in the Sm_2O_3 content in the initial mixture. Along with the obtained values of the enthalpy of α→β phase transitions in lithium ferrite, the high Curie temperatures indicate that the main product in all synthesized samples was the ordered α-$Li_{0.5}Fe_{2.5}O_4$ phase. Sintering at elevated temperature resulted in a slight decrease in the content of the $SmFeO_3$ phase and an increase in the lithium ferrite phase. As confirmed by the reduced values of the Curie temperature and the phase transition enthalpy, the sample not modified with samarium contained a significant amount of the disordered β-$Li_{0.5}Fe_{2.5}O_4$ phase. The introduction of samarium ions at the synthesis stage led to the preservation of the ordered α-$Li_{0.5}Fe_{2.5}O_4$ phase during sintering, whose morphology depends on the concentration of the secondary phase $SmFeO_3$. In the case of the introduction of a low concentration of Sm_2O_3 (up to 4.7 wt %), the structure of the samples was characterized by the presence of more regular polyhedral grains. In this case, the density of the samples insignificantly decreased while maintaining a high Curie temperature corresponding to unsubstituted lithium ferrite. The obtained results can support future more detailed studies of the electromagnetic properties of lithium ferrites modified with low concentrations of REEs in the microwave range.

Acknowledgments

The work was supported by the Ministry of Science and Higher Education of the Russian Federation within the framework of the State Assignment in the Field of Scientific Activity (project FSWW-2023-0011).

Authors' contributions

E.N. Lysenko—research idea, analyzing and discussing the results, and editing the text of the article.

V.A. Vlasov—development of a methodology for conducting the experiment, participation in experimental work, discussion of the results, and writing and formatting the text of the article.

Yu.S. Elkina—participation in experiments, processing the obtained data, search for scientific publications on the topic of the article, formation of the list of references, and participation in editing the text of the article.

A.P. Surzhikov—setting up and planning experiments, and discussion of the results.

The authors declare no conflicts of interest.

REFERENCES

1. Trukhanov A.V., Tishkevich D.I., Timofeev A.V., *et al.* Structural and electrodynamic characteristics of the spinel-based composite system. *Ceram. Int.* 2024;50(12): 21311–21317. https://doi.org/10.1016/j.ceramint.2024.03.241
2. Kostishin V.G., Vergazov R.M., Menshova S.B., Isaev I.M. Prospects for the use of ferrites with high magnetic permeability and permittivity as radio-absorbing materials. *Russ. Technol. J.* 2020;8(6):87–108 (in Russ.). https://doi.org/10.32362/2500-316X-2020-8-6-87-108
3. Kostishin V.G., Isaev I.M., Salogub D.V. Radio-Absorbing Magnetic Polymer Composites Based on Spinel Ferrites: A Review. *Polymers*. 2024;16(7):1003. https://doi.org/10.3390/polym16071003
4. Sherstyuk D.P., Starikov A.Yu., Zhivulin V.E., Zherebtsov D.A., Mikhailov G.G., Vinnik D.A. Study of the effect of cobalt substitution on the structure of nickel-zinc ferrite. *Vestnik Yuzhno-Ural'skogo gosudarstvennogo universiteta. Seriya: Metallurgiya = Bulletin of the South Ural State University. Ser. Metallurgy*. 2020;20(2):51–56 (in Russ.). https://doi.org/10.14529/met200205
5. Nikishina E.E. Heterophase synthesis of cobalt ferrite. *Tonk. Khim. Tekhnol. = Fine Chem. Technol*. 2021;16(6):502–511. https://doi.org/10.32362/2410-6593-2021-16-6-502-511
6. Gavrilova M.A., Gavrilova D.A., Kondrashkova I.S., Krasilin A.A. Formation of $Zn_{0.5}Ni_{0.5}Fe_2O_4$ Nanocrystals in Conditions of Solution Combustion: Effect of the Type of Fuel on the Structure and Morphology. *Fizika i khimiya stekla*. 2023;49(4):459–470 (in Russ.). https://doi.org/10.31857/S013266512260090X
7. Ahmad M., Shahid M., Alanazi Y.M., ur Rehman A., Asif M., Dunnill C.W. Lithium ferrite ($Li_{0.5}Fe_{2.5}O_4$): synthesis, structural, morphological and magnetic evaluation for storage devices. *J. Mater. Res. Technol*. 2022;18:3386–3395. https://doi.org/10.1016/j.jmrt.2022.03.113
8. Askarzadeh N., Shokrollahi H. A review on synthesis, characterization and properties of lithium ferrites. *Results in Chemistry.* 2024;10:101679. https://doi.org/10.1016/j.rechem.2024.101679
9. Nikolaeva S.A., Lysenko E.N., Nikolaev E.V., Vlasov V.A., Surzhikov A.P. Microstructure and electromagnetic properties of $Li_{0.65}Fe_{1.6}Ti_{0.5}Zn_{0.2}Mn_{0.05}O_4$–$Bi_2O_3$–$ZrO_2$ composite ceramics. *J. Alloy. Compd*. 2023;941:169025. https://doi.org/10.1016/j.jallcom.2023.169025
10. Lysenko E., Nikolaev E., Vlasov V., Surzhikov A. Microstructure and reactivity of Fe_2O_3-Li_2CO_3-ZnO ferrite system ball-milled in a planetary mill. *Thermochim. Acta*. 2018; 664:100–107. https://doi.org/10.1016/j.tca.2018.04.015

СПИСОК ЛИТЕРАТУРЫ

1. Trukhanov A.V., Tishkevich D.I., Timofeev A.V., *et al.* Structural and electrodynamic characteristics of the spinel-based composite system. *Ceram. Int.* 2024;50(12):21311–21317. https://doi.org/10.1016/j.ceramint.2024.03.241
2. Костишин В.Г., Вергазов Р.М., Меньшова С.Б., Исаев И.М. Перспективы применения ферритов с высокими значениями магнитной и диэлектрической проницаемостей в качестве радиопоглощающих материалов. *Russ. Technol. J.* 2020;8(6):87–108. https://doi.org/10.32362/2500-316X-2020-8-6-87-108
3. Kostishin V.G., Isaev I.M., Salogub D.V. Radio-Absorbing Magnetic Polymer Composites Based on Spinel Ferrites: A Review. *Polymers*. 2024;16(7):1003. https://doi.org/10.3390/polym16071003
4. Шерстюк Д.П., Стариков А.Ю., Живулин В.Е., Жеребцов Д.А., Михайлов Г.Г., Винник Д.А. Изучение влияния замещения кобальтом на структуру никель-цинкового феррита. *Вестник Южно-Уральского государственного университета. Серия: Металлургия*. 2020;20(2):51–56. https://doi.org/10.14529/met200205
5. Никишина Е.Е. Гетерофазный синтез феррита кобальта. *Тонкие химические технологии*. 2021;16(6):502–511. https://doi.org/10.32362/2410-6593-2021-16-6-502-511
6. Гаврилова М.А., Гаврилова Д.А., Кондрашкова И.С., Красилин А.А. Формирование нанокристаллов $Zn_{0.5}Ni_{0.5}Fe_2O_4$ в условиях растворного горения: влияние типа "топлива" на структуру и морфологию. *Физика и химия стекла*. 2023;49(4):459–470. https://doi.org/10.31857/S013266512260090X
7. Ahmad M., Shahid M., Alanazi Y.M., ur Rehman A., Asif M., Dunnill C.W. Lithium ferrite ($Li_{0.5}Fe_{2.5}O_4$): synthesis, structural, morphological and magnetic evaluation for storage devices. *J. Mater. Res. Technol*. 2022;18:3386–3395. https://doi.org/10.1016/j.jmrt.2022.03.113
8. Askarzadeh N., Shokrollahi H. A review on synthesis, characterization and properties of lithium ferrites. *Results in Chemistry.* 2024;10:101679. https://doi.org/10.1016/j.rechem.2024.101679
9. Nikolaeva S.A., Lysenko E.N., Nikolaev E.V., Vlasov V.A., Surzhikov A.P. Microstructure and electromagnetic properties of $Li_{0.65}Fe_{1.6}Ti_{0.5}Zn_{0.2}Mn_{0.05}O_4$–$Bi_2O_3$–$ZrO_2$ composite ceramics. *J. Alloy. Compd*. 2023;941:169025. https://doi.org/10.1016/j.jallcom.2023.169025
10. Lysenko E., Nikolaev E., Vlasov V., Surzhikov A. Microstructure and reactivity of Fe_2O_3-Li_2CO_3-ZnO ferrite system ball-milled in a planetary mill. *Thermochim. Acta*. 2018; 664:100–107. https://doi.org/10.1016/j.tca.2018.04.015

11. Martinson K.D., Ivanov A.A., Panteleev I.B., *et al.* Pre-Ceramic Nanostructured Liznmn-Ferrite Powders: Synthesis, Structure, and Electromagnetic Properties. *Glass and Ceramics*. 2020;77(5–6):215–220. https://doi.org/10.1007/s10717-020-00274-9
[Original Russian Text: Martinson K.D., Ivanov A.A., Panteleev I.B., Popkov V.I. Pre-Ceramic Nanostructured LiZnMn-Ferrite Powders: Synthesis, Structure, and Electromagnetic Properties. *Steklo i keramika*. 2020;6:16–23 (in Russ.).]
12. Isaev I.M., Kostishin V.G., Korovushkin V.V., *et al.* Crystal chemistry and magnetic properties of polycrystalline spinel ferrites $Li_{0.33}Fe_{2.29}Zn_{0.21}Mn_{0.17}O_4$. *Russ. J. Inorg. Chem.* 2021;66(12):1917–1924. https://doi.org/10.1134/S0036023621120056
[Original Russian Text: Isaev I.M., Kostishin V.G., Korovushkin V.V., Shipko M.N., Timofeev A.V., Mironovich A.Yu., Salogub D.V., Shakirzyanov R.I. Crystal chemistry and magnetic properties of polycrystalline spinel ferrites $Li_{0.33}Fe_{2.29}Zn_{0.21}Mn_{0.17}O_4$. *Zhurnal neorganicheskoi khimii*. 2021;66(12):1792–1800 (in Russ.). https://doi.org/10.31857/S0044457X21120059]
13. Mahmoudi M., Kavanlouei M., Maleki-Ghaleh H. Effect of composition on structural and magnetic properties of nanocrystalline ferrite $Li_{0.5}Sm_xFe_{2.5-x}O_4$. *Powd. Metal. Metal. Ceram.* 2015;54:31–39. https://doi.org/10.1007/s11106-015-9676-9
14. Slimani Y., Almessiere M.A., Güner S., Kurtan U., Shirsath S.E., Bayka A., Ercan I. Magnetic and microstructural features of Dy^{3+} substituted $NiFe_2O_4$ nanoparticles derived by sol–gel approach. *J. Sol-Gel Sci. Techn*. 2020;95:202–210. https://doi.org/10.1007/s10971-020-05292-1
15. Jacob B.P., Thankachan S., Xavier S., Mohammed E.M. Effect of Tb^{3+} substitution on structural, electrical and magnetic properties of sol–gel synthesized nanocrystalline nickel ferrite. *J. Alloys Compd.* 2013;578:314–319. https://doi.org/10.1016/j.jallcom.2013.04.147
16. Heiba Z.K., Mohamed M.B., Arda L., Dogan N. Cation distribution correlated with magnetic properties of nanocrystalline gadolinium substituted nickel ferrite. *Magn. Magn. Mater.* 2015;391:195–202. https://doi.org/10.1016/j.jmmm.2015.05.003
17. Ahmad S.I., Ansari S.A., Kumar D.R. Structural, morphological, magnetic properties and cation distribution of Ce and Sm co-substituted nano crystalline cobalt ferrite. *Mater. Chem. Phys.* 2018;208:248–257. https://doi.org/10.1016/j.matchemphys.2018.01.050
18. Nikumbh A.K., Pawar R.A., Nighot D.V., Gugale G.S., Sangale M.D., Khanvilkar M.B., Nagawade A.V. Structural, electrical, magnetic and dielectric properties of rare-earth substituted cobalt ferrites nanoparticles synthesized by the co-precipitation method. *Magn. Magn. Mater.* 2014;355:201–209. https://doi.org/10.1016/j.jmmm.2013.11.052
19. Ahmad I., Abbas T., Ziya A.B., Maqsood A. Structural and magnetic properties of erbium doped nanocrystalline Li–Ni ferrites. *Ceram. Int.* 2014;40(6):7941–7945. https://doi.org/10.1016/j.ceramint.2013.12.142
20. Junaid M., Khan M.A., Iqbal F., Murtaza G., Akhtar M.N., Ahmad M., Shakir I., Warsi M.F. Structural, spectral, dielectric and magnetic properties of Tb–Dy doped Li-Ni nano-ferrites synthesized via microemulsion route. *Magn. Magn. Mater.* 2016;419:338–344. https://doi.org/10.1016/j.jmmm.2016.06.043
11. Мартинсон К.Д., Иванов А.А., Пантелеев И.Б., Попков В.И. Предкерамические наноструктурированные порошки LiZnMn-феррита: получение, структура и электромагнитные свойства. *Стекло и керамика*. 2020;6:16–23.
12. Исаев И.М., Костишин В.Г., Коровушкин В.В., Шипко М.Н., Тимофеев А.В., Миронович А.Ю., Салогуб Д.В., Шакирзянов Р.И. Кристаллохимия и магнитные свойства поликристаллических ферритов-шпинелей $Li_{0.33}Fe_{2.29}Zn_{0.21}Mn_{0.17}O_4$. *Журн. неорган. химии.* 2021;66(12):1792–1800. https://doi.org/10.31857/S0044457X21120059
13. Mahmoudi M., Kavanlouei M., Maleki-Ghaleh H. Effect of composition on structural and magnetic properties of nanocrystalline ferrite $Li_{0.5}Sm_xFe_{2.5-x}O_4$. *Powd. Metal. Metal. Ceram.* 2015;54:31–39. https://doi.org/10.1007/s11106-015-9676-9
14. Slimani Y., Almessiere M.A., Güner S., Kurtan U., Shirsath S.E., Bayka A., Ercan I. Magnetic and microstructural features of Dy^{3+} substituted $NiFe_2O_4$ nanoparticles derived by sol–gel approach. *J. Sol-Gel Sci. Techn*. 2020;95:202–210. https://doi.org/10.1007/s10971-020-05292-1
15. Jacob B.P., Thankachan S., Xavier S., Mohammed E.M. Effect of Tb^{3+} substitution on structural, electrical and magnetic properties of sol–gel synthesized nanocrystalline nickel ferrite. *J. Alloys Compd.* 2013;578:314–319. https://doi.org/10.1016/j.jallcom.2013.04.147
16. Heiba Z.K., Mohamed M.B., Arda L., Dogan N. Cation distribution correlated with magnetic properties of nanocrystalline gadolinium substituted nickel ferrite. *Magn. Magn. Mater.* 2015;391:195–202. https://doi.org/10.1016/j.jmmm.2015.05.003
17. Ahmad S.I., Ansari S.A., Kumar D.R. Structural, morphological, magnetic properties and cation distribution of Ce and Sm co-substituted nano crystalline cobalt ferrite. *Mater. Chem. Phys.* 2018;208:248–257. https://doi.org/10.1016/j.matchemphys.2018.01.050
18. Nikumbh A.K., Pawar R.A., Nighot D.V., Gugale G.S., Sangale M.D., Khanvilkar M.B., Nagawade A.V. Structural, electrical, magnetic and dielectric properties of rare-earth substituted cobalt ferrites nanoparticles synthesized by the co-precipitation method. *Magn. Magn. Mater.* 2014;355:201–209. https://doi.org/10.1016/j.jmmm.2013.11.052
19. Ahmad I., Abbas T., Ziya A.B., Maqsood A. Structural and magnetic properties of erbium doped nanocrystalline Li–Ni ferrites. *Ceram. Int.* 2014;40(6):7941–7945. https://doi.org/10.1016/j.ceramint.2013.12.142
20. Junaid M., Khan M.A., Iqbal F., Murtaza G., Akhtar M.N., Ahmad M., Shakir I., Warsi M.F. Structural, spectral, dielectric and magnetic properties of Tb–Dy doped Li-Ni nano-ferrites synthesized via microemulsion route. *Magn. Magn. Mater.* 2016;419:338–344. https://doi.org/10.1016/j.jmmm.2016.06.043
21. Al-Hilli M.F., Li S., Kassim K.S. Structural analysis, magnetic and electrical properties of samarium substituted lithium–nickel mixed ferrites. *Magn. Magn. Mater*. 2012;324(5):873–879. https://doi.org/10.1016/j.jmmm.2011.10.005
22. Li D.-Y., Sun Y.-K., Xu Y., Ge H.-L., Wu Q., Yan C. Effects of Dy^{3+} substitution on the structural and magnetic properties of $Ni_{0.5}Zn_{0.5}Fe_2O_4$ nanoparticles prepared by a sol-gel self-combustion method. *Ceram. Int.* 2015;41(3B):4581–4589. https://doi.org/10.1016/j.ceramint.2014.11.156

21. Al-Hilli M.F., Li S., Kassim K.S. Structural analysis, magnetic and electrical properties of samarium substituted lithium–nickel mixed ferrites. *Magn. Magn. Mater*. 2012;324(5):873–879. https://doi.org/10.1016/j.jmmm.2011.10.005
22. Li D.-Y., Sun Y.-K., Xu Y., Ge H.-L., Wu Q., Yan C. Effects of Dy^{3+} substitution on the structural and magnetic properties of $Ni_{0.5}Zn_{0.5}Fe_2O_4$ nanoparticles prepared by a sol-gel self-combustion method. *Ceram. Int.* 2015;41(3B):4581–4589. https://doi.org/10.1016/j.ceramint.2014.11.156
23. Zhao L., Yang H., Yu L., Cui Y., Feng S. Effects of Gd_2O_3 on structure and magnetic properties of Ni–Mn ferrite. *J. Mater. Sci*. 2006;41:3083–3087. https://doi.org/10.1007/s10853-005-1545-3
24. Almessiere M.A., Slimani Y., Guner S., Nawaz M., Baykal A., Aldakheel F., Sadaqat A., Ercan I. Effect of Nb substitution on magneto-optical properties of $Co_{0.5}Mn_{0.5}Fe_2O_4$ nanoparticles. *J. Mol. Struct.* 2019;1195:269–279. https://doi.org/10.1016/j.molstruc.2019.05.075
25. Lin Q., Yuan G., He Y., Wang L., Dong J., Yu Y. The Influence of La-substituted $Cu_{0.5}Co_{0.5}Fe_2O_4$ nanoparticles on its structural and magnetic properties. *Mater. Des.* 2015;78:80–84. https://doi.org/10.1016/j.matdes.2015.04.029
26. Lysenko E.N., Vlasov V.A., Nikolaeva S.A., Nikolaev E.V. TG, DSC, XRD, and SEM studies of the substituted lithium ferrite formation from milled Sm_2O_3/Fe_2O_3/Li_2CO_3 precursors. *J. Therm. Anal. Calorim.* 2023;148:1445–1453. https://doi.org/10.1007/s10973-022-11665-1
27. Ridley D.H., Lessoff H., Childress J.D. Effect of lithium and oxygen losses on magnetic and crystallographic properties of spinel lithium ferrite. *J. Am. Ceram. Soc.* 1970;53(6):304–311. https://doi.org/10.1111/j.1151-2916.1970.tb12113.x
28. Surzhikov A.P., Frangulyan T.S., Ghyngazov S.A., Lysenko E.N. Investigation of structural states and oxidation processes in $Li_{0.5}Fe_{2.5}O_{4-\delta}$ using TG analysis. *J. Therm. Anal. Calorim.* 2012;108:1207–1212. https://doi.org/10.1007/s10973-011-1734-z
29. Lysenko E.N., Malyshev A.V., Vlasov V.A., Nikolaev E.V., Surzhikov A.P. Microstructure and thermal analysis of lithium ferrite pre-milled in a high-energy ball mill. *J. Therm. Anal. Calorim.* 2018;134:127–133. https://doi.org/10.1007/s10973-018-7549-4.
30. Berbenni V., Marini A., Capsoni D. Solid state reaction study of the system Li_2CO_3/Fe_2O_3. *Z. Naturforschung – Sect. J. Phys. Sci.* 1998;53:997–1003. https://doi.org/10.1515/zna-1998-1212
31. An S.Y., Shim I.B., Kim C.S. Synthesis and magnetic properties of $LiFe_5O_8$ powders by a sol–gel process. *Magn. Magn Mater.* 2005;290–291:1551–1554. https://doi:10.1016/j.jmmm.2004.11.244
32. Mazen S.A., Abu-Elsaad N.I. Characterization and magnetic investigations of germanium-doped lithium ferrite. *Ceram. Int.* 2014;40:11229–11237. https://doi.org/10.1016/j.ceramint.2014.03.167
33. Ahniyaz A., Fujiwara T., Song S.-W., Yoshimura M. Low temperature preparation of β-$LiFe_5O_8$ fine particles by hydrothermal ball milling. *J. Solid State Ion.* 2002;151:419–423. https://doi.org/10.1016/S0167-2738(02)00548-9

23. Zhao L., Yang H., Yu L., Cui Y., Feng S. Effects of Gd_2O_3 on structure and magnetic properties of Ni–Mn ferrite. *J. Mater. Sci*. 2006;41:3083–3087. https://doi.org/10.1007/s10853-005-1545-3
24. Almessiere M.A., Slimani Y., Guner S., Nawaz M., Baykal A., Aldakheel F., Sadaqat A., Ercan I. Effect of Nb substitution on magneto-optical properties of $Co_{0.5}Mn_{0.5}Fe_2O_4$ nanoparticles. *J. Mol. Struct.* 2019;1195:269–279. https://doi.org/10.1016/j.molstruc.2019.05.075
25. Lin Q., Yuan G., He Y., Wang L., Dong J., Yu Y. The Influence of La-substituted $Cu_{0.5}Co_{0.5}Fe_2O_4$ nanoparticles on its structural and magnetic properties. *Mater. Des.* 2015;78:80–84. https://doi.org/10.1016/j.matdes.2015.04.029
26. Lysenko E.N., Vlasov V.A., Nikolaeva S.A., Nikolaev E.V. TG, DSC, XRD, and SEM studies of the substituted lithium ferrite formation from milled Sm_2O_3/Fe_2O_3/Li_2CO_3 precursors. *J. Therm. Anal. Calorim.* 2023;148:1445–1453. https://doi.org/10.1007/s10973-022-11665-1
27. Ridley D.H., Lessoff H., Childress J.D. Effect of lithium and oxygen losses on magnetic and crystallographic properties of spinel lithium ferrite. *J. Am. Ceram. Soc.* 1970;53(6):304–311. https://doi.org/10.1111/j.1151-2916.1970.tb12113.x
28. Surzhikov A.P., Frangulyan T.S., Ghyngazov S.A., Lysenko E.N. Investigation of structural states and oxidation processes in $Li_{0.5}Fe_{2.5}O_{4-\delta}$ using TG analysis. *J. Therm. Anal. Calorim.* 2012;108:1207–1212. https://doi.org/10.1007/s10973-011-1734-z
29. Lysenko E.N., Malyshev A.V., Vlasov V.A., Nikolaev E.V., Surzhikov A.P. Microstructure and thermal analysis of lithium ferrite pre-milled in a high-energy ball mill. *J. Therm. Anal. Calorim.* 2018;134:127–133. https://doi.org/10.1007/s10973-018-7549-4.
30. Berbenni V., Marini A., Capsoni D. Solid state reaction study of the system Li_2CO_3/Fe_2O_3. *Z. Naturforschung – Sect. J. Phys. Sci.* 1998;53:997–1003. https://doi.org/10.1515/zna-1998-1212
31. An S.Y., Shim I.B., Kim C.S. Synthesis and magnetic properties of $LiFe_5O_8$ powders by a sol–gel process. *Magn. Magn Mater.* 2005;290–291:1551–1554. https://doi:10.1016/j.jmmm.2004.11.244
32. Mazen S.A., Abu-Elsaad N.I. Characterization and magnetic investigations of germanium-doped lithium ferrite. *Ceram. Int.* 2014;40:11229–11237. https://doi.org/10.1016/j.ceramint.2014.03.167
33. Ahniyaz A., Fujiwara T., Song S.-W., Yoshimura M. Low temperature preparation of β-$LiFe_5O_8$ fine particles by hydrothermal ball milling. *J. Solid State Ion.* 2002;151:419–423. https://doi.org/10.1016/S0167-2738(02)00548-9

About the authors

Elena N. Lysenko, Dr. Sci. (Eng.), Professor, Head of the Laboratory, Research Laboratory for Electronics, Semiconductors and Dielectrics, Research School of High-Energy Physics, Tomsk Polytechnic University (30, Lenina pr., Tomsk, 634034, Russia). E-mail: lysenkoen@tpu.ru. Scopus Author ID 25027787100, ResearcherID K-1582-2013, RSCI SPIN-code 6536-9390, https://orcid.org/0000-0002-5093-2207

Vitaly A. Vlasov, Cand. Sci. (Phys.-Math.), Senior Researcher, Research Laboratory for Electronics, Semiconductors and Dielectrics, Research School of High-Energy Physics, Tomsk Polytechnic University (30, Lenina pr., Tomsk, 634034, Russia). E-mail: vlvitan@tpu.ru. Scopus Author ID 7202194125, ResearcherID K-1257-2013, RSCI SPIN-code 2003-8431, https://orcid.org/0000-0002-5946-2117

Yuliya S. Elkina, Postgraduate Student, Engineer, Research Laboratory for Electronics, Semiconductors and Dielectrics, Research School of High-Energy Physics, Tomsk Polytechnic University (30, Lenina pr., Tomsk, 634034, Russia). E-mail: ysm7@tpu.ru. Scopus Author ID 58892380200, ResearcherID HHS-0003-2022, RSCI SPIN-code 6717-1540, https://orcid.org/0000-0002-2708-9872

Anatoly P. Surzhikov, Dr. Sci. (Phys.-Math.), Professor, Head of the Department, Division for Testing and Diagnostics, School of Non-Destructive Testing, Tomsk Polytechnic University (30, Lenina pr., Tomsk, 634034, Russia). E-mail: surzhikov@tpu.ru. Scopus Author ID 6603494148, ResearcherID K-1224-2013, RSCI SPIN-code 1875-0293, https://orcid.org/0000-0003-2795-398X

Об авторах

Лысенко Елена Николаевна, д.т.н., профессор, заведующая лабораторией, Проблемная научно-исследовательская лаборатория электроники диэлектриков и полупроводников, Исследовательская школа физики высокоэнергетических процессов, ФГАОУ ВО «Национальный исследовательский Томский политехнический университет» (634050, Россия, г. Томск, пр-т Ленина, д. 30). E-mail: lysenkoen@tpu.ru. Scopus Author ID 25027787100, ResearcherID K-1582-2013, SPIN-код РИНЦ 6536-9390, https://orcid.org/0000-0002-5093-2207

Власов Виталий Анатольевич, к.ф.-м.н., старший научный сотрудник, Проблемная научно-исследовательская лаборатория электроники диэлектриков и полупроводников, Исследовательская школа физики высокоэнергетических процессов, ФГАОУ ВО «Национальный исследовательский Томский политехнический университет» (634050, Россия, г. Томск, пр-т Ленина, д. 30). E-mail: vlvitan@tpu.ru. Scopus Author ID 7202194125, ResearcherID K-1257-2013, SPIN-код РИНЦ 2003-8431, https://orcid.org/0000-0002-5946-2117

Елькина Юлия Сергеевна, аспирант, инженер, Проблемная научно-исследовательская лаборатория электроники диэлектриков и полупроводников, Исследовательская школа физики высокоэнергетических процессов, ФГАОУ ВО «Национальный исследовательский Томский политехнический университет» (634050, Россия, г. Томск, пр-т Ленина, д. 30). E-mail: ysm7@tpu.ru. Scopus Author ID 58892380200, ResearcherID HHS-0003-2022, SPIN-код РИНЦ 6717-1540, https://orcid.org/0000-0002-2708-9872

Суржиков Анатолий Петрович, д.ф.-м.н., профессор, заведующий кафедрой – руководитель отделения на правах кафедры, Отделение контроля и диагностики, Инженерная школа неразрушающего контроля и безопасности, ФГАОУ ВО «Национальный исследовательский Томский политехнический университет» (634050, Россия, г. Томск, пр-т Ленина, д. 30). E-mail: surzhikov@tpu.ru. Scopus Author ID 6603494148, ResearcherID K-1224-2013, SPIN-код РИНЦ 1875-0293, https://orcid.org/0000-0003-2795-398X

Translated from Russian into English by V. Glyanchenko
Edited for English language and spelling by Thomas A. Beavitt